Rheological Behavior and in Situ Confocal Imaging of Bijels Made by Mixing

Rheological Behavior and in-situ Confocal Imaging of Bijels Made by Mixing

Katherine A. Macmillan,[†,§] John Royer,[†] Alexander Morozov,[†] Yogesh M. Joshi,[‡] Michel Cloitre,[¶] and Paul S. Clegg[*,†]

†*School of Physics and Astronomy, University of Edinburgh, James Clerk Maxwell Building, Peter Guthrie Tait Road, Edinburgh, EH9 3FD, UK*

‡*Department of Chemical Engineering, Indian Institute of Technology Kanpur, Kanpur 208016, India*

¶*Molecular, Macromolecular Chemistry, and Materials, CNRS, ESPCI Paris, PSL Research University, 10 rue Vauquelin, 75005 Paris, France*

§*Née Rumble*

E-mail: paul.clegg@ed.ac.uk

Abstract

Bijels (bicontinuous interfacially jammed emulsion gels) have the potential to be useful in many different applications due to their internal connectivity and the possibility of efficient mass transport through the channels. Recently new methods of making the bijel have been proposed which simplify the fabrication process making commercial application more realistic. Here we study the flow properties of bijels prepared by mixing alone using oscillatory rheology combined with confocal microscopy and also squeezing flow experiments. We found that the bijel undergoes a two-step yielding process where the first step corresponds to the fluidizing of the interface allowing motion of the structure and the second step corresponds to the breaking of the structure. In

the squeeze flow experiments, the yield stress of the bijel is observed to show a power law dependence on squeezing speed. However, when stress in excess of yield stress is plotted against shear rate, all the different squeeze flow data show a superposition.

Keywords

Bijels, Bicontinuous, Emulsions, Mechanical properties, Rheo-imaging, Two-step yielding, Squeezing flow

Introduction

Bijels are solid-stabilized emulsions with bicontinuous tortuous domains.[1] A bicontinuous structure is particularly attractive because it can have a large surface area of interface packed within a small volume which is advantageous for uses such as catalysts and electrodes for batteries and fuel cells.[2–5] Additionally, it has also been proposed that bijels could be used as scaffolds for tissue engineering, controlled release vehicles, cross flow microreactors or separation processors.[1,3,6–8] In order to realize some of these applications, one of the liquid phases of the bijel has been polymerized to create a bicontinuous polymer scaffold.[2,3] This polymer structure can then be used as a template for creating bicontinuous structures out of other materials and some experimentally realized examples include ceramics and metals.[2,3,9] The polymer templating method has been used to successfully produce a $Ni/Ni(OH)_2$ composite electrode from a bijel scaffold.[5]

The first method developed for fabricating bijels harnessed the phase separation of partially miscible liquids via spinodal decomposition to create a bicontinuous arrangement of fluid domains which then became particle-stabilized.[6,8] Unfortunately there are two major problems with this method: firstly that neutrally wetting particles are required and secondly that the choice of liquids is limited to pairs of partially miscible liquids with symmetric phase diagrams and similar densities.[8,10,11] This has led to several investigations into different so-

lutions to these problems including the use of mixtures of commercially available particles as stabilizers[12] and the use of a ternary solute in order to induce the phase separation of two immiscible liquids.[13] Recently two new methods for making bijels simply by mixing were proposed which circumvent both the problems mentioned above.[11,14] These methods involved using both surfactants and particles as interface stabilizers and have the benefit that, with a straightforward method of fabrication and the possibility of using functional nanoparticles as stabilizers, they could more easily be deployed in applications.[11,14] (The downside of no longer using partially miscible liquids is that temperature can no longer be used to control interfacial tension and hence the elastic properties of the structure.[1,3]) One of the new methods used low viscosity liquids and two types of surfactants in order to induce a bicontinuous structure.[14] The other method involved using high viscosity liquids and a two-step mixing protocol in order to form the bicontinuous structure.[11,15] This latter method, described by Cai *et al.*, will be used to form bijels for the experiments performed in this work.[11]

Before any type of bijel can be utilized in specific applications, the mechanical properties must be examined in order to ensure that the structure can withstand processing conditions and use.[10] Furthermore, understanding the connection between the macroscopic material properties of the bijel and the changes to the microstructure is important because this will aid designing a material with the desired properties.[16] Various attempts have been made in order to elucidate these properties for the original bijel[6–8,17,18] and polymeric bicontinuous structures.[19–23] Previous studies of bijels prepared via phase separation have demonstrated that the composite has a yield stress.[6,7,18] A lower bound on the value of the yield stress was estimated using a falling wire to be approximately 600 Pa for a water–2,6-lutidine bijel stabilized by silica particles with an interface separation of approximately 40 μm.[6] The internal yield stress of the deformation of the microstructure of an ethanediol–nitromethane bijel with an interface separation of approximately 30 μm was found to be approximately 4000 Pa using centrifugal compression experiments.[18] For the bijel made by direct mixing, the rheological properties could additionally help reveal the origins of its stability.[24]

In this study we investigate the rheological properties of bijels made by directly mixing glycerol, silicone oils, silica particles and cetyltrimethylammonium bromide (CTAB) surfactant. First we discuss the results of a rotational shear experiment followed by those from oscillatory shear rheology combined with confocal microscopy imaging. For the oscillatory shear experiments first frequency sweeps are analyzed with comparisons to frequency sweeps for other bicontinuous structures. Next the two-step yielding observed in the amplitude sweeps is discussed and the confocal microscopy images are used to characterize the associated changes in microstructure. Afterwards, squeeze flow experiments are carried out at a series of fixed plate speeds using bijel samples of fixed volume. The squeezing behavior is analyzed by using a no slip model of Herschel-Bulkley flow in order to create flow curves. The combination of rheological approaches (oscillating shear and squeeze flow) has made it possible for us to understand the rate-dependent yielding behavior of our composite material.

Results and discussion

The bicontinuous structure formed by two-step mixing of glycerol, silicone oils, CTAB and silica nanoparticles at our chosen composition has tortuous domains of approximately 100 - 200 μm stabilized by both particles and surfactant molecules, see Supporting Information Movie S1. In this study we investigate some of the rheological properties of this bijel using oscillatory rheology combined with confocal imaging and squeeze flow rheology. For the original bijels (prepared via phase separation induced by a temperature quench) these experiments are difficult to perform because the structure is fragile. Indeed, fabrication via a controlled temperature quench on a rheometer is in itself challenging. It is more straightforward to perform rheological experiments with the bijel made by direct mixing because it can be scooped out with a spatula without destroying the structure. Since scooping is likely to have modified the structure, we check that the morphology remains that of a bijel on the rheo-imaging set-up as the measurements are carried out.

Rheo-imaging Experiments

Rheo-imaging experiments were performed with the bijels fabricated using the method described in the Experimental Section (following Cai *et al.*[11]) beginning with rotational shear (from a shear rate of $0.1\,s^{-1}$ to $100\,s^{-1}$) which demonstrated that the structure undergoes shear thinning (see Figure 1a).The flow curve is reasonably well described by the Herschel-Bulkley model (dashed line). At high shear rates the viscosity approaches a plateau at approximately 1 Pa s which is between the measured viscosities of the silicone oil mix (1.28 ± 0.01 Pa s) and the glycerol (0.64 ± 0.02 Pa s). The confocal microscopy images taken during the rotational shear experiment show that the structure rapidly began to break apart. Uneven particle-stabilized structures were observed to form first and, as the shear rate was increased, large fully separated domains of glycerol and silicone oil were observed (see Figures 1b, 1c and 1d). This is consistent with the observations of Cai *et al.* who found that further fast mixing of the formed bijel destroyed the bicontinuous structure leading to the formation of droplets.[11] The viscosity as a function of shear rate was measured a second time, immediately following the first study (again from a shear rate of $0.1\,s^{-1}$ to $100\,s^{-1}$). There is a clear decrease in viscosity at low shear rate reflecting the destruction of the structure (see Figure 1). At higher shear rates the viscosity meets the data from the first shear experiment indicating the point at which the structure had previously been destroyed.

Next, frequency sweeps and amplitude sweeps were performed in combination with confocal microscopy with a parallel plate geometry at a 1 mm plate separation. Figure 2 shows frequency sweeps for three samples at 0.1 % strain, which is in the linear viscoelastic region (see Figure 3). There is significant sample-to-sample variability in spite of the samples having identical composition. This presumably reflects very slight differences in preparation procedures, handling conditions or both. In all three cases, the bijel displays solid-like behavior at low frequencies because the storage modulus is much higher than the loss modulus. The storage modulus was observed to remain higher than the loss modulus at all but a few high frequencies for all three samples. Both moduli also increased in value with increasing

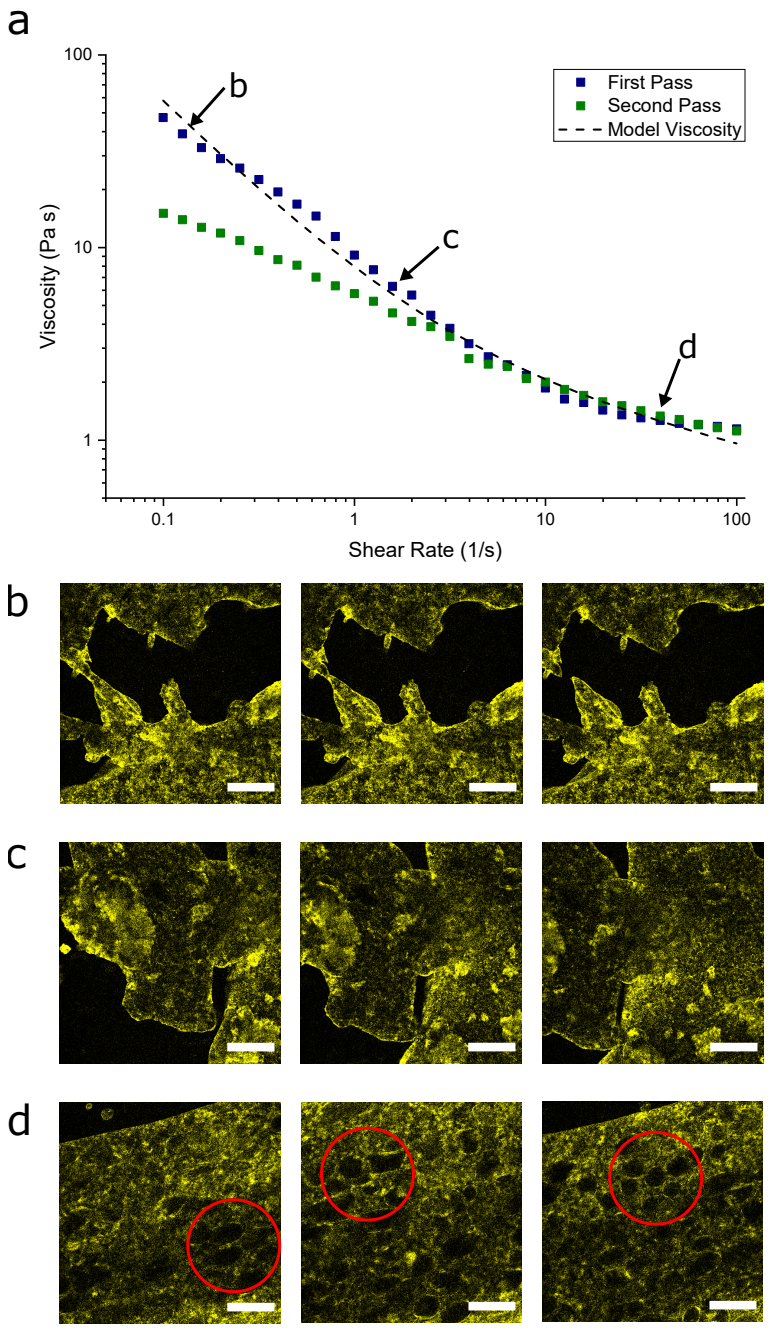

Figure 1: **a**: A graph of viscosity versus shear rate for a bijel sample where the second experiment is performed on the same bijel directly after the first. The dashed line corresponds to the Herschel-Bulkley model with $\sigma_0 = 5.3\,\mathrm{Pa}$, $K = 2.6\,\mathrm{Pa\ s}^n$ and $n = 0.77$. **b**: A series of confocal microscopy images of the sample at $0.13\,\mathrm{s}^{-1}$. **c**: A series of confocal microscopy images of the sample at $1.59\,\mathrm{s}^{-1}$. **d**: A series of confocal microscopy images of the sample at $39.81\,\mathrm{s}^{-1}$. Red circles highlight droplets. In all images only the FITC-labeled particles are shown (yellow), the scale bars are $200\,\mu\mathrm{m}$ and the series last three seconds.

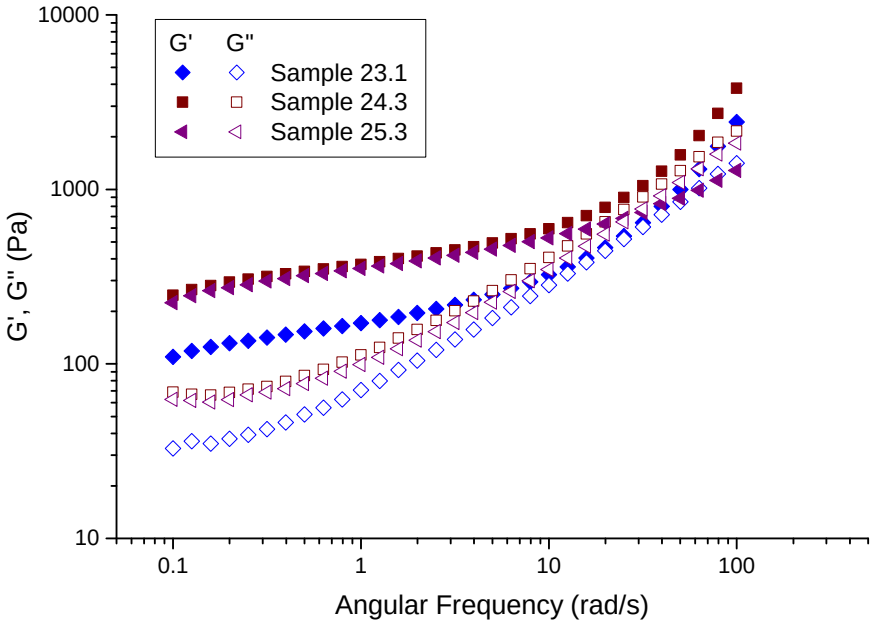

Figure 2: A graph showing the changes in the storage modulus (G' closed symbols) and the loss modulus (G'' open symbols) with angular frequency for three bijel samples with identical composition at 0.1 % strain.

frequency, which suggests that there is a contribution from fast relaxation modes that may be related to the particle dynamics at the interface. The influence of particle dynamics may be particularly relevant for this bijel because the particles stabilizing the interface may not be completely jammed. The confocal images show that all three samples have tortuous arrangements of liquid domains but the associated moduli indicate that there is noticeable sample-to-sample variation.

Frequency sweeps of co-continuous polymer blends stabilized by graphene particles were observed to have similarly shaped curves of the storage and loss moduli as those found here. The gel-like behavior, particularly a plateau at low frequencies, was attributed to the network of graphene particles at the interface of the bicontinuous structure.[25] In our study, it is difficult to conclusively determine from Figure 2 whether a plateau at low frequencies was present. Similar behavior of the storage and loss moduli with increasing frequency was also observed for a silica nanoparticle-stabilized low molecular weight polybutene and styrene trimer bijel, a silica nanoparticle-stabilized co-continuous polymer blend and a bicontinuous

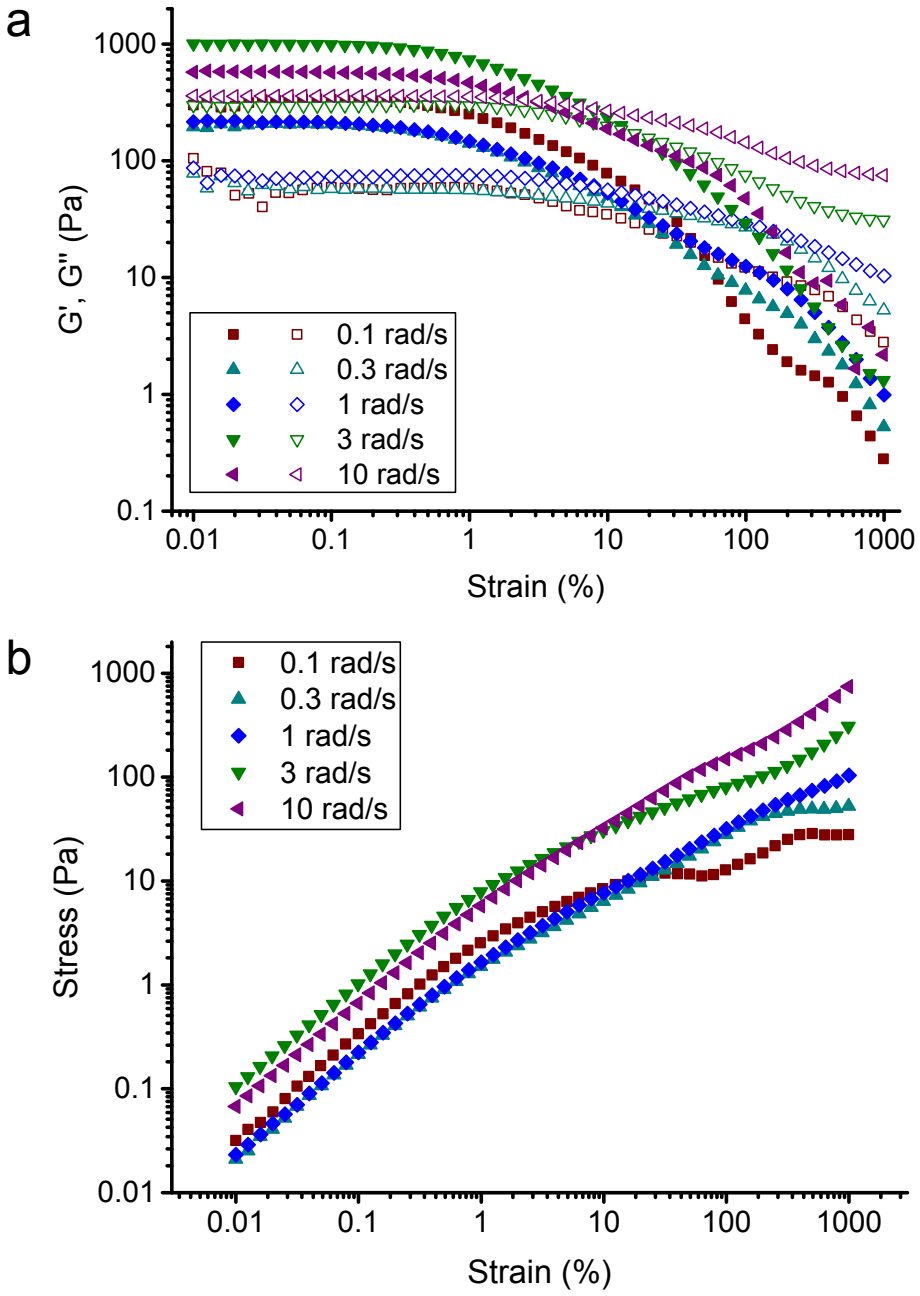

Figure 3: **a**: A graph showing the changes in the storage modulus (G' closed symbols) and the loss modulus (G'' open symbols) with strain for bijel samples at different angular frequencies. **b**: A graph showing the changes in the shear stress with the strain. Each different angular frequency study was carried out on a separate bijel sample.

structure with one phase packed with silica particles made from a ternary blend of two polymers.[17,22,23] Therefore, it is possible that this frequency response may be observed for a broad class of bicontinuous structures.

Directly after the frequency sweep was performed, an amplitude sweep from 0.01 – 1000 % strain was performed at one of five different angular frequencies. The resulting storage and loss moduli are plotted against strain in Figure 3a and the shear stress is plotted against strain in Figure 3b. Initially, for all angular frequencies, the linear viscoelastic region is observed where the storage modulus and the loss modulus show a constant value in a limit of small strains. It can be seen that in the linear response regime, the storage modulus is higher than the loss modulus (see Figure 3a). This regime is also observed in the stress versus strain graph where, at low strain, the stress increases approximately linearly with the strain (see Figure 3b). This indicates that at low strain the bijel made by direct mixing displays solid-like behavior. However, with increasing strain, both moduli start to decrease and cross over and the gradient in the stress curve changes: at higher strain the material departs from linearity and then begins to yield. The onset of the non-linear response begins at a stress $\sim 1\,\mathrm{Pa}$ and the moduli cross over at a stress $\sim 15\,\mathrm{Pa}$. Neither of these values show a systematic trend with frequency, however, the values can vary by about a factor of 2 between different samples.

The moduli versus strain curves show that the bijel exhibits two-step yielding (see Figure 3a) indicating that there are two distinct changes in the system associated with the bijel starting to flow. The first step occurs as the system leaves the linear viscoelastic region and the second step occurs at much higher strain and stress. The second step is very prominent at lower measurement frequencies; at higher frequencies it is sometimes observed as a shoulder in the storage modulus. In the stress against strain graph these two steps appear as two changes in the gradient of the curve and the data from the experiments using lower frequencies also show plateau regions (see Figure 3b). Two-step yielding behavior has been observed in a variety of other colloidal systems.[24,26–33] In some of these examples the storage modulus and loss modulus were observed to cross only after both steps indicating that both are required to induce liquid-like behavior.[26,27] By contrast, Figure 3a shows that for the bijel made by mixing, the cross over point of the storage modulus and loss modulus

occurred before the second yielding step indicating that the dissipation of energy over a single cycle becomes large between the two yielding processes (see Figure 3a).

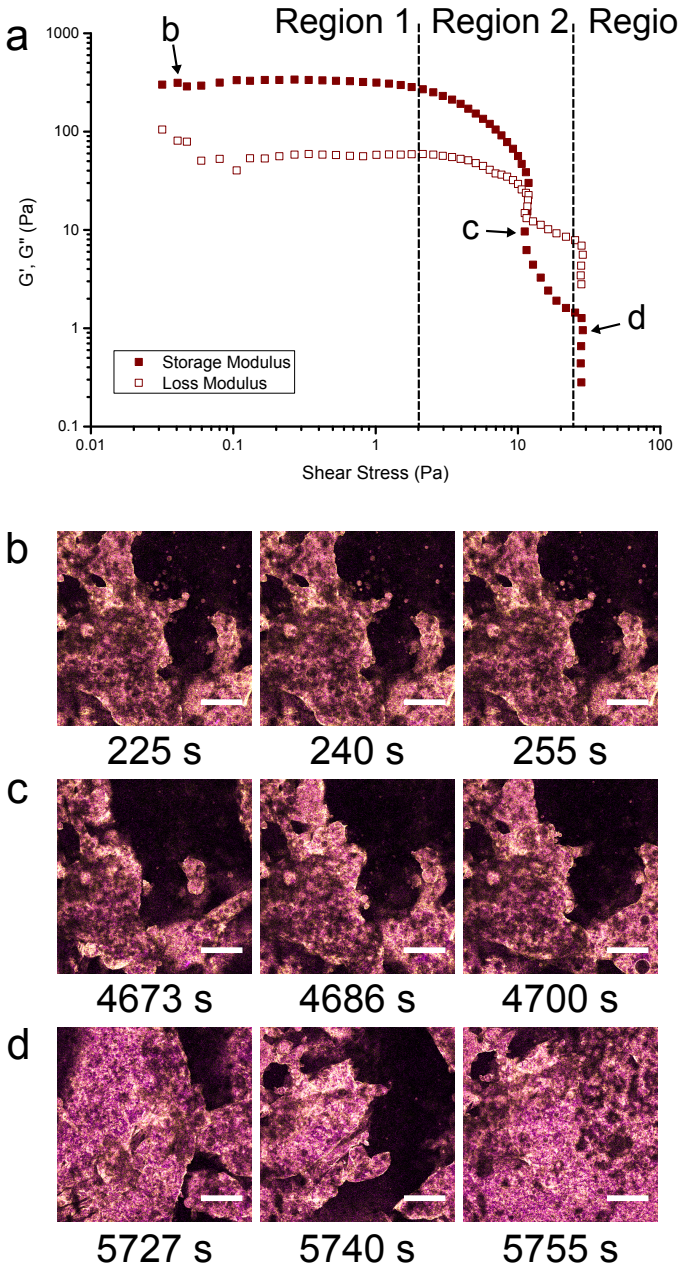

Figure 4: **a**: A graph showing the changes in the storage modulus (G') and the loss modulus (G'') with shear stress for a bijel sample undergoing oscillations at a frequency of 0.1 rad/s. **b**: Confocal microscopy images of the sample at 0.04 Pa. **c**: Confocal microscopy images of the sample at 11.61 Pa. **d**: Confocal microscopy images of the sample at 28.53 Pa. In all images, the FITC-labeled particles are colored yellow, the nile red-labeled glycerol is colored magenta, the scale bars are 200 μm and the times are relative to the start of the application of shear.

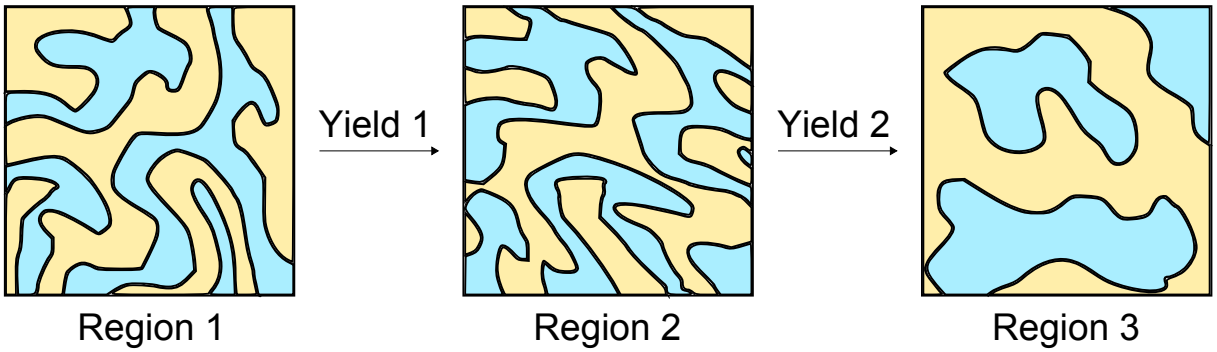

Figure 5: A diagram showing the changes in the structure of the bijel in the two-step yielding process. Yield 1 corresponds to deformation whilst yield 2 involves break-up of the interfaces. The image for region 2 roughly corresponds to a vertical gradient direction and a horizontal flow direction.

For the different systems which display two-step yielding, the behavior has often been associated with structures at two distinct length scales.[24,26–33] In our experiments, the different mechanisms that could occur at each of the two yielding steps were investigated by collecting confocal microscopy images of the samples during the amplitude sweeps. Confocal microscopy images approximately 80 μm from the glass plate at the base of the sample at different points in the oscillation of the bijel under three different stresses are shown in Figure 4 with the corresponding amplitude sweep performed at a frequency of 0.1 rad/s. The structure was not observed to move at all at this depth in the linear viscoelastic region apart from the sedimentation or creaming of unconnected droplets (see Figure 4b). Unreversed motion in three dimensions began to be observed after the first yielding step but the domains remained connected together (see Figure 4c). This indicates that the interface must be stretched and compressed at different places in the structure during this phase. The increasing strain on the interface during this process then leads to the structure breaking up into individual large domains which was observed at the second yielding step. These large uneven structures then became more rounded with increasing stress (see Figure 4d). The structure is not observed to heal after the second yielding, hence, the breaking up process is an irreversible reorganization of the sample. The behavior is shown schematically in Figure 5.

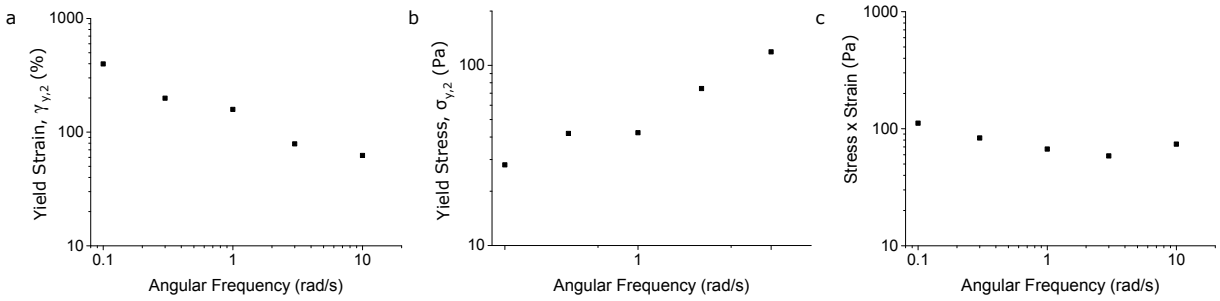

Figure 6: Graphs showing **a**: the changes in the strain at the second yield point with the angular frequency; **b**: the changes in the shear stress at the second yield point with the angular frequency; **c**: that the product of the stress and the strain at the second yield point varies little with the angular frequency.

The frequency dependence (or lack thereof) of the complex bijel yielding behavior is a very important aspect of the oscillating shear rheology results. The strain at the first yielding point and at the cross over of the moduli displayed no dependence on the angular frequency. By contrast, the strain value at the second yielding point was found to decrease with increasing frequency and the stress value at the second yielding point was observed to increase with increasing angular frequency (see Figures 3 and 6). This means, when subjected to faster oscillations, a smaller movement of the bijel is required in order for yielding, and therefore bijel break up, to occur. Conversely, the stress at the second yielding point increases with increasing angular frequency meaning more stress is required to induce yielding at the lower strains. Figure 6c shows that the product of the stress and the strain at the second yielding point remains fairly constant with increasing angular frequency. Given that there is some variation between the bijel structures, the product remains constant with increasing angular frequency at a value of $\sim 100\,\mathrm{J/m^3}$. This is of the same order of magnitude as the interfacial tension divided by the interface separation: the threshold that must be exceeded to finally disrupt the interfaces.

Squeeze-flow Experiments

Squeeze flow experiments were performed at the ESPCI in Paris on bijels with the same composition but which were prepared using a slightly different mixing protocol. These experiments were undertaken to establish the behavior under destructive testing.[34] First a frequency sweep from 100 rad/s to 0.1 rad/s at 0.1 % strain at a 1 mm plate separation was performed. Next, squeezing experiments were carried out at a variety of squeezing velocities from a 1 mm plate separation to a 0.25 mm plate separation. In order to remain in the constant volume limit, the final gap size was chosen so that the sample always remained within the area of the plates. The final part of the experimental protocol involved a second frequency sweep from 100 rad/s to 0.1 rad/s at the new plate separation. The values of the moduli produced by the rheometer were corrected to account for the change in contact area between the plate and the sample. Before the squeezing experiments were performed, confocal microscopy images were taken of the bijels in order to ascertain the initial structure and these were repeated after the squeezing experiments when the sample had been unloaded.

Figure 7a shows the resulting moduli of frequency sweeps performed at 0.1 % strain before and after the squeezing experiment. First the frequency sweeps can be compared to those performed during the rheo-imaging experiments (see Figure 2). For both experiments the storage modulus is higher than the loss modulus at low frequencies indicating solid-like behavior and both moduli increase with increasing frequency. The values of the moduli are approximately the same at low angular frequency for the bijel in Figure 7a and sample 23.1 in Figure 2. Despite this, the moduli do not increase as rapidly with increasing frequency in the experiments conducted in Paris (see Figure 7a) as was observed during the rheo-imaging experiments performed in Edinburgh (see Figure 2). It is most likely that this difference occurs because the particles were less well dispersed for the Paris experiments (see Methods Section); the bijel structures were stabilized by *fluffy* clusters of particles resulting in lower connectivity and gaps in the interfacial coverage.

Secondly, the frequency sweeps made before squeezing and after squeezing can be com-

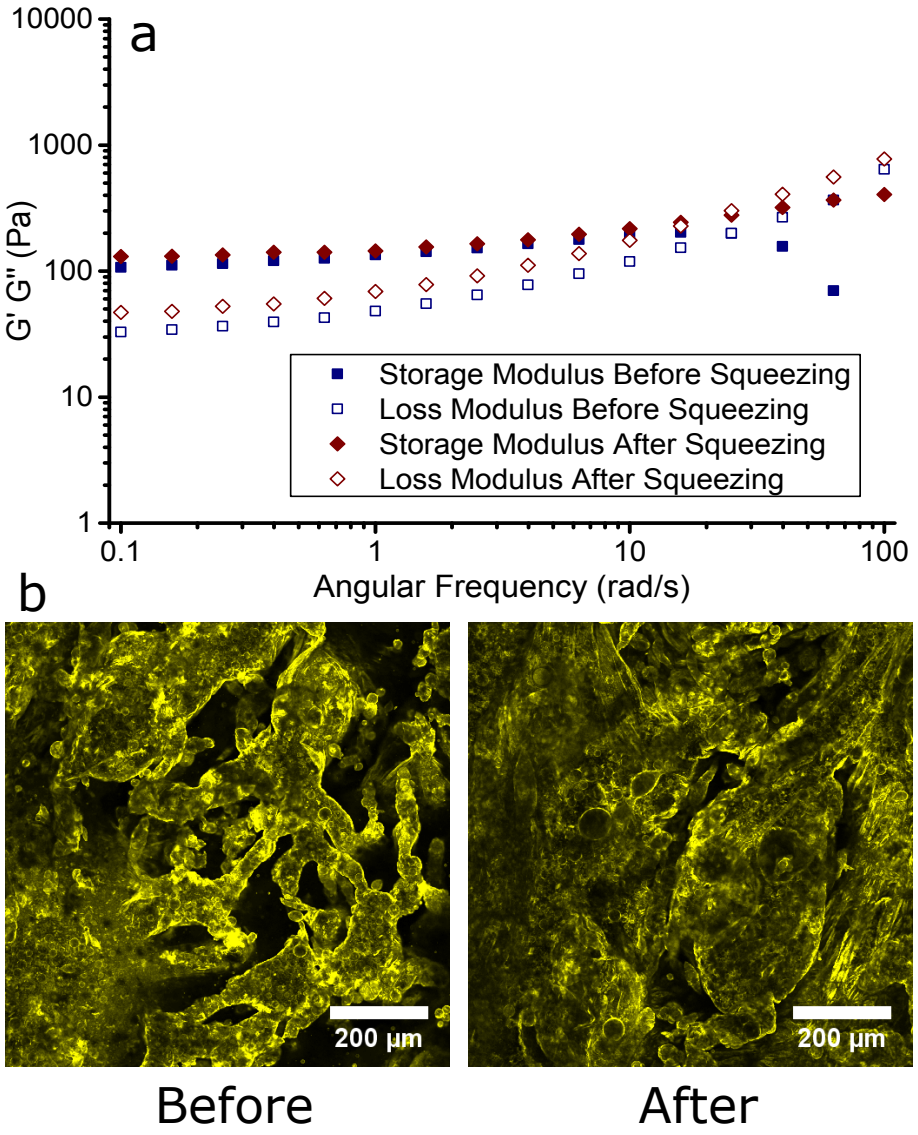

Figure 7: (a) A graph showing the changes in the storage modulus (G') and the loss modulus (G'') with angular frequency at 0.1 % strain before and after squeezing for a bijel sample. (b) Example confocal microscopy images taken of a bijel before and after the squeezing experiment where the FITC-labeled particles are colored yellow.

pared (see Figure 7a). The frequency sweeps before and after squeezing are reasonably similar which indicates that the linear response of the bijel is not greatly modified by the squeeze flow protocol (see Figure 7a). However, the confocal images indicate that the structure has been destroyed after squeezing and unloading (N.B. raising the geometry and transferring a sample to a microscope slide could in itself be destructive, see Figure 7b). Given that very

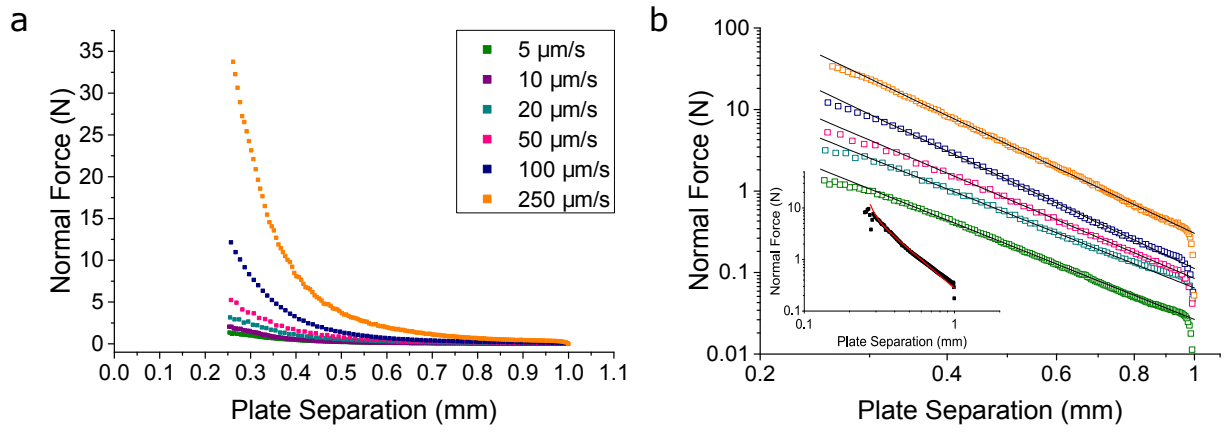

Figure 8: Graphs showing the changes in the normal force with plate separation for a variety of squeezing velocities for bijel samples: (a) the raw data and (b) a log-log plot of the normal force versus plate separation including simple power law fits. Inset: showing the change in the normal force with plate separation for the sample data compressed at a squeezing velocity of 10 μm/s and the corresponding Herschel-Bulkley fit described in the text.

little change in the frequency sweeps was observed and in the first set of experiments the bijel structure was still observed to be intact after the plate was lowered, it is likely that the observed destruction actually occurred during the raising of the geometry.

During the squeezing experiments at constant plate speed, the normal force was measured and this is plotted against the plate separation in Figure 8a. Clearly, the force required to maintain the constant velocity increases as the plate separation decreases. On a log-log plot it is evident that the normal force grows as a power law for much of the experiment (see Figure 8b). The fitted exponents are all less than -3 with some falling below -3.6. Such a strong growth in normal force with decreasing plate separation is consistent with the lack of wall-slip in our experiments.[35] In the absence of slip, shear flow dominates the response to squeezing.

The shear stress and shear strain can be calculated from these measurements by assuming an underlying model which we begin by taking to be the Herschel-Bulkley model:

$$\sigma = \sigma_0 + K\dot{\epsilon}^n \tag{1}$$

where σ is the shear stress, σ_0 is the yield stress, K is the consistency, n is the exponent and $\dot{\epsilon}$ is the shear rate (defined[36] for values of $\sigma > \sigma_0$). This is motivated by existing observations of a bijel yield stress[6,8,18] together with shear thinning behavior (see Figure 1). The force required to squeeze a Herschel-Bulkley fluid at constant velocity under no slip conditions has been calculated for constant area experiments where the volume of material decreases as the plate separation decreases.[37,38] The resulting force equation was found by combining the method of Covey and Stanmore[37] with that of Adams *et al.*[38] to give

$$F = \frac{2\sigma_0 \pi R^3}{3h} + \frac{2\pi K R^{n+3}}{(n+3)} \left(\frac{2n+1}{n} \right)^n \frac{(-\dot{h})^n}{h^{2n+1}} \tag{2}$$

as the final result.[39] Here R is the radius of the circular area being squeezed and h is the plate separation. The experiments performed here, however, used the fixed volume approach whereby the area being squeezed increases as the plate separation decreases. The force equation can be easily modified from fixed area to fixed volume using the relation

$$R = R_0 \sqrt{\frac{h_0}{h}}$$

where R_0 is the initial radius of the circular area before squeezing and h_0 is the initial plate separation.[40] The normal force measured when squeezing a Herschel-Bulkley fluid at constant velocity in constant volume experiments is then given by

$$F = \frac{2\sigma_0 V^{3/2}}{3h^{5/2}\pi^{1/2}} + \frac{2KV^{(n+3)/2}}{(n+3)\pi^{(n+1)/2}} \left(\frac{2n+1}{n} \right)^n \frac{(-\dot{h})^n}{h^{(5n+5)/2}} \tag{3}$$

where $V = \pi R_0^2 h_0$ is the fixed volume of the sample.

Equation 3 can be used to fit the curves of experimental normal force against the plate separation for all six different squeezing velocities. These fits were performed between the step in the curve from the onset of squeezing and up to the point where an obvious knee appears. This is because the behavior of the sample at the onset of squeezing reflects the complexities of yielding and is difficult to analyze. Likewise for the very smallest plate

separations a single shear stress can correspond to more than one shear strain which is beyond our simple model. It is possible that this indicates that some material was escaping from the plates.[41] The fitting data for one example curve (squeezing velocity 10 μm/s) for the bijel samples is shown inset to Figure 8b. In spite of all of the samples being of the same material, we have found that it is not possible to fit all of the data taken using different plate speeds with a single set of σ_0, K and n values via Equation 3. The flow properties depend on the plate speed in a manner that is not captured by the Herschel-Bulkley model. Based on our preceding oscillatory shear studies, we assume that this complication reflects a dependence of the yield stress on the speed of deformation. Hence we have modified Equation 3 to include a power law dependence of the yield stress on the plate speed.

$$F = \frac{2S_0(-\dot{h})^p V^{3/2}}{3h^{5/2}\pi^{1/2}} + \frac{2KV^{(n+3)/2}}{(n+3)\pi^{(n+1)/2}}\left(\frac{2n+1}{n}\right)^n \frac{(-\dot{h})^n}{h^{(5n+5)/2}} \tag{4}$$

The best fit parameters are a prefactor $S_0 = 3240$ Pa $(\mathrm{m/s})^{-p}$ and a plate speed exponent $p = 0.601$. With this additional feature it is now possible to model all of the data using a single set of best fit parameters.

Table 1: Showing the values of the parameters σ_0, K and n obtained from fitting the squeezing data for the bijel samples using Equation 3 modified by the power law variation of the yield stress (Equation 4). A single optimal set of values of S_0, p, K and n were found for all data sets simultaneously. Hence, K and n are constant whereas σ_0 has a power law dependence on the plate speed. The best fit from Fig. 1 is also included for comparison.

Sample	σ_0 Pa	K Pa s^n	n –
Bijel 5 $\mu m/s$	2.12	2.25	0.70
Bijel 10 $\mu m/s$	3.21	2.25	0.70
Bijel 20 $\mu m/s$	4.87	2.25	0.70
Bijel 50 $\mu m/s$	8.44	2.25	0.70
Bijel 100 $\mu m/s$	12.8	2.25	0.70
Bijel 250 $\mu m/s$	22.2	2.25	0.70
Figure 1a	5.34	2.61	0.77

The best fit values of K, σ_0 and n are given in Table 1. The bijel samples can be described as shear thinning because the exponent n is less than one indicating that as the shear rate

increases, the increase in the shear stress decreases. This is in agreement with experiments described earlier in this study which also found that the bijel made by mixing displayed shear thinning behavior (see Figure 1a). The corresponding values from the Herschel-Bulkley model are in reasonable agreement (Table 1).

In order to create flow curves, the shear rate and the shear stress at the edge of the sample were determined. The equation for the shear rate at the edge of the sample is

$$\dot{\epsilon} = \left(\frac{2n+1}{n}\right)\left(\frac{V^{1/2}(-\dot{h})}{\pi^{1/2}h^{5/2}}\right) \tag{5}$$

which is a little different to that used previously for a power law fluid,[19] see Appendix A. The shear stress at the edge can then easily be calculated to be

$$\sigma_e = -\frac{n}{3}\sigma_0 + \left(\frac{n+3}{2}\right)\left(\frac{\pi^{1/2}h^{5/2}F}{V^{3/2}}\right) \tag{6}$$

which is again derived in Appendix A. Once the values of the shear rate and the shear stress have been calculated for each plate separation, flow curves of shear stress versus shear rate can be created as shown in Figure 9a.

Figure 9 demonstrates that the flow curves recorded at different plate speeds share a common power law growth in shear stress but are systematically offset from one another due to the dependence of the yield stress on the plate speed. The value of the yield stress is shown as a single triangle offset from the corresponding data set. By subtracting the yield stress from each measured set of data, we observe the results collapsing to form a single curve. These flow curves imply that the bijel is a shear thinning fluid which exhibits a small yield stress that is dependent on the speed of deformation.

In our oscillating shear experiments it is possible to resolve two different yielding steps and how their characteristics change with the oscillation frequency. In the squeeze flow study the sample experiences a range of shear rates simultaneously and we find that we are unable to resolve the details of the yielding process. The sample undergoes destructive testing; the

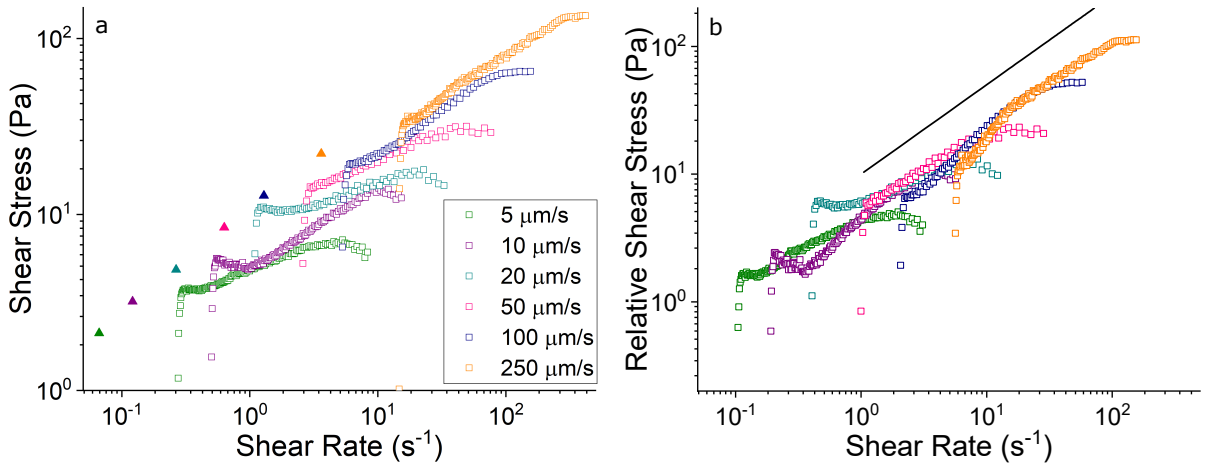

Figure 9: Graphs showing the changes in the shear stress with shear rate at various squeezing velocities for the bijel samples (a) the full curves with the contribution due to the yield stress indicated as a triangle (b) the flow curves with the yield stress subtracted showing a common power law trend (solid line with exponent 0.7).

resulting normal force is consistent with a yield stress which is weakly frequency dependent. This is similar to the second yielding step in the oscillating shear study.

These results provide insight into the nature of the new bijel material and how it differs from bijels prepared via phase separation. The value of the yield stress obtained in this study is one – two orders of magnitude smaller than that hypothesized for the original bijel[6] and a further order of magnitude smaller than that obtained for internal yielding of the bicontinuous microstructure in centrifugal compression.[18] This discrepancy could exist because the particles at the interface of the bijel made by mixing have unconventional jamming characteristics due to the additional presence of surfactants. Another important factor, which could cause this discrepancy, is the larger domain sizes of the bijels made by mixing.

Conclusions

Before the bijel can be made into products, it is necessary to determine how the structure will behave under processing conditions and during use. An understanding of how the macroscopic properties are linked to the microstructure will also make it possible to engineer

the desired properties for a given application. The bijel prepared by mixing is shear thinning with complex yielding behavior. It was found that this particular bijel exhibits two-step yielding in response to an oscillating sweep of the shear amplitude. The structure started to move and the particle-stabilized interface was distorted at the first yielding step but the domains remained connected to each other. The structure was broken up at the second yielding step and the large pieces started to move independently of each other.

The results from the the squeeze flow experiments indicate that under compression the bijel made by mixing has only a modest yield stress. Yielding in squeezing compression is only observed to occur in a single step which may well be a consequence of the range of conditions which exist between the plates at any moment during the experiment. In comparison to the small yield stress obtained here, the yield stress hypothesized for the original bijel was much larger[6] and the value of the stress at which the microstructure of the original bijel yields is also at significantly larger stress values.[18] This difference has been attributed to the combination of particles and surfactants at the interface of the bijel made by mixing, which means that the surfactant molecules modify the contacts between jammed particles, resulting in a more flexible interface. The mixed bijels are hence softer and easier to scoop and spread.

Experimental

Materials

Ethanol (puriss), silicone oil (10,000 cSt), silicone oil (50 cSt) and nile red (for microscopy) were purchased from Sigma-Aldrich. Glycerol (laboratory reagent grade $\geq$98 %) and cetyltrimethylammonium bromide (CTAB) (Pure) were purchased from Fisher Chemical. All chemicals were used as received. The silica particles (radius 14 nm) were made via the Stöber method by Andrew Schofield and fluorescently labeled with fluorescein isothiocyanate (FITC) dye (isomer I, Sigma-Aldrich) as described by Imhof *et al.*[42,43]

Methods

Bijel Fabrication

Bijels were fabricated using the mixing process reported by Cai *et al.*[11] Silica particles with a radius of 14 nm, labeled with FITC and dispersed in ethanol at a known mass fraction were first weighed into a vial followed by nile red-labeled glycerol in order to obtain 3 g of 1 wt% silica particles in glycerol. The mixture was sonicated using an ultrasonic probe (Sonics Vibracell VCX500) at an amplitude of 20 % in a 5 seconds on, 5 seconds off cycle for a total of 5 minutes. The ethanol in the silica particles in glycerol dispersion was then evaporated off by leaving the sample in a Binder oven set to 60 °C or a Memment oven set to 50 °C overnight. Immediately after this, 8 mg of CTAB was weighed out into a new vial followed by 0.6 g of the silica particles in glycerol dispersion which leads to the mass ratio of 3:4 (particles:CTAB). The mixture was stirred at 200 rpm for 5 minutes using a magnetic stirrer bar and a magnetic stirrer plate (IKA RCT basic). Next 0.5 g of a 1:1 (by mass) mixture of silicone oils (50 cSt and 10,000 cSt) was added to the vial. The mixture was then stirred slowly at 200 rpm for 1 minute (IKA RCT basic magnetic stirrer plate), rested for two minutes (no mixing) and then mixed quickly for another five minutes (at level 2 on a Stuart stir CB161 magnetic stirrer plate). A stack of images of a bijel as a function of depth is shown in the Supporting Information as Movie S1.

For the squeeze flow experiments performed at the ESPCI in Paris a slightly different mixing protocol for making the bijels was used. First, the amount of the 1 wt% silica in glycerol dispersion was increased to 17 g. Second, the 1 wt% silica in glycerol dispersion was not used immediately but seven days later and over the course of a further ten days. Third, the magnetic stirring plate used for the slow mixing step was changed to a VELD scientific AREX DIGITAL PRO heating magnetic stirrer and the mixing speed increased to 250 rpm. Finally, the fast mixing step was reduced to only three minutes as opposed to the original five minutes and the resting step was skipped.

Rheology

In Edinburgh, an Anton Paar rheometer (MCR 301) was combined with a Leica (DMi8 TCS SP8) confocal microscope in order to perform rheology experiments whilst simultaneously imaging the structure. A roughened parallel plate geometry with a diameter of 25 mm and a plate separation of 1 mm was used to perform the experiments. The samples were loaded onto the base glass plate using a spatula and the parallel plate brought up to contact with the bijel, then lowered down at a speed of approximately 100 μm/s, reduced to 25 μm/s over the last 1 mm of compression. Confocal microscopy was performed using the 488 nm and 552 nm lasers to excite the FITC-labeled particles and the nile red-labeled glycerol respectively. Time series confocal microscopy images were taken in conjunction with the rheology experiments. No pre-shear was carried out in advance of any of our rheology studies. For every sample first a frequency sweep from 0.1 rad/s to 100 rad/s at 0.1 % strain was performed. Next an amplitude sweep from 0.01 % strain to 1000 % at various frequencies was performed. A rotational shear experiment from a shear rate of 0.1 s^{-1} to 100 s^{-1} was also performed with a cone plate geometry with a roughened 25 mm diameter cone with an angle of 1°. Additionally, the viscosity of the glycerol and the silicone oil mix was determined with a rotational shear experiment from a shear rate of 0.01 s^{-1} to 100 s^{-1} using a cone-plate geometry with a slightly roughened 50 mm cone at an angle of 1° on the same rheometer.

In Paris, an Anton Paar rheometer (PHYSICA 502) with a disposable parallel plate geometry was used in order to perform squeeze flow experiments. Glass slides were affixed to the surface of the top and bottom 50 mm parallel plates and the temperature at the bottom plate was set to 25 °C. The samples were loaded onto the base glass plate using a small spatula and the parallel plate was lowered down to a plate separation of 1 mm. No-slip boundary conditions were observed at the glass surfaces. Here a frequency sweep from 100 to 0.1 rad/s at 0.1 % strain was performed. A constant volume approach was used for the squeezing experiments and these were performed at six different squeezing velocities from a plate separation of 1 mm to 0.25 mm. A second frequency sweep from 100 to 0.1 rad/s at

0.1 % strain was then performed. The values given by the rheometer for the moduli during the second frequency sweep were divided by 4 (the value of the difference in the radius of the cylinder of sample squared) to correct for the larger area in contact with the geometry after the squeezing experiment. Before the sample was loaded and after the experiment was finished a small sample was taken, placed on a glass cover slide and observed using a Karl Zeiss LSM510 confocal microscope with the 488 nm laser for imaging the FITC-labeled silica particles.

Appendix A Derivation of the stress at the plate edge

Here we briefly outline the details of the calculation that yields Eqs.(2-5) of the main text. First, we consider the constant area squeeze flow, and then reformulate the results obtained for the constant volume case.

We consider a fluid confined between two circular plates that move towards each other along the direction perpendicular to the plates. We introduce a cylindrical polar coordinate system (r, θ, z) with the z-axis chosen perpendicular to the plates. Following Covey and Stanmore,[37] we measure $z \in [0, h/2]$ from the lower plate, with $z = h/2$ corresponding to the middle plane of the sample. The stress and velocity fields are assumed to be symmetric with respect to the $z = h/2$-plane.

In the absence of inertia and normal stresses, the rz-component of the Navier-Stokes equation reduces to

$$-\frac{\partial P(r)}{\partial r} + \frac{\partial \sigma}{\partial z} = 0, \tag{A.1}$$

which can be integrated[37] to yield

$$\sigma = -\frac{\partial P(r)}{\partial r}\left(\frac{h}{2} - z\right). \tag{A.2}$$

The fluid is assumed to obey the Herschel-Bulkley model, Eq.(1), and yields when the shear stress σ exceeds the yield-stress value σ_0. This condition defines a non-trivial surface $z_y = z_y(r)$ that separates the moving fluid, $z < z_y$, from the unyielded material, $z \leq z_y$. Combining Eq.(A.2) with Eq.(1) we obtain

$$z_y(r) = \frac{h}{2} - \sigma_0 \left(\frac{\partial P(r)}{\partial r} \right)^{-1}. \tag{A.3}$$

The velocity of the moving fluid obeys

$$\sigma_0 + K \left(\frac{\partial v_r}{\partial z} \right)^n = -\frac{\partial P(r)}{\partial r} \left(\frac{h}{2} - z \right), \tag{A.4}$$

with the boundary condition $v_r(0) = 0$, which is solved by

$$\begin{aligned} v_r(z) = & \frac{n}{n+1} \left(\frac{\partial P(r)}{\partial r} \right)^{-1} \frac{1}{K^{1/n}} \\ & \times \left[\left\{ -\frac{\partial P(r)}{\partial r} \frac{h}{2} - \sigma_0 \right\}^{\frac{n+1}{n}} - \left\{ -\frac{\partial P(r)}{\partial r} \left(\frac{h}{2} - z \right) - \sigma_0 \right\}^{\frac{n+1}{n}} \right]. \end{aligned} \tag{A.5}$$

The unyielded region moves with the velocity given by $v_r(z_y)$. As shown by Convey and Stanmore, the pressure gradient is determined from the mass conservation condition: The volume decrease of a cylindrical fluid element with the radius r due to the plates approaching each other with the velocity $-\dot{h}$ is balanced by the outflow of the material thorough the side surface of the cylinder. For a cylindrical element centred around the origin this gives

$$\pi r^2 \left(-\dot{h} \right) = 4\pi r \left[\int_0^{z_y} dz v_r(z) + v_r(z_y) \left(\frac{h}{2} - z_y \right) \right], \tag{A.6}$$

or, after integration,

$$-\frac{n+1}{n}\frac{\dot{h}\,K^{1/n}}{h^2\sigma_0^{1/n}}\left(\frac{h}{2\sigma_0}\frac{\partial P(r)}{\partial r}\right)^2 r-\frac{n+1}{2n+1}\left(-\frac{h}{2\sigma_0}\frac{\partial P(r)}{\partial r}-1\right)^{\frac{2n+1}{n}} -\left(-\frac{h}{2\sigma_0}\frac{\partial P(r)}{\partial r}-1\right)^{\frac{n+1}{n}}=0. \tag{A.7}$$

Eq.(A.7) is strongly non-linear and cannot be solved analytically for the pressure gradient. Instead, Adams et al.[38] developed a uniform approximation to its solution given by

$$\frac{h}{2\sigma_0}\frac{\partial P(r)}{\partial r}\approx -1-\left(\frac{2n+1}{n}\right)^n\frac{r^n(-\dot{h})^nK}{h^{2n}\sigma_0}, \tag{A.8}$$

that, together with the boundary condition $p(R)=0$, where R is the size of the plate, results in

$$P(r)=\frac{2\sigma_0}{h}\left[R-r+\left(\frac{2n+1}{n}\right)^n\frac{(-\dot{h})^nK}{h^{2n}\sigma_0}\frac{R^{n+1}-r^{n+1}}{n+1}\right]. \tag{A.9}$$

Finally, the force F that needs to be applied to both plates to sustain the flow is given by

$$F=2\pi\int_0^R dr\,r\,P(r)=\frac{2\pi\sigma_0R^3}{3h}+\frac{2\pi KR^{n+3}}{n+3}\left(\frac{2n+1}{n}\right)^n\frac{(-\dot{h})^n}{h^{2n+1}}, \tag{A.10}$$

which is Eq.(2) of the main text, and also agrees with the result of Adams et al.[38] The shear rate at the edge of the sample, $\dot{\epsilon}$, can readily be evaluated

$$\dot{\epsilon}\equiv\left.\frac{\partial v_r}{\partial z}\right|_{r=R}=\frac{2n+1}{n}\frac{R\left(-\dot{h}\right)}{h^2}, \tag{A.11}$$

and the corresponding shear stress at the edge is given by

$$\sigma_e=-\frac{n\sigma_0}{3}+\frac{n+3}{2\pi}\frac{h}{R^3}F. \tag{A.12}$$

As discussed in the main text, to recast these result into the form applicable under the constant-volume conditions, we observe that at all times the current height and radius of the sample should satisfy

$$\pi R^2 h = V, \tag{A.13}$$

where V is the sample's original volume. Using $R = \sqrt{V/\pi h}$ in Eqs.(A.4)-(A.6), we obtain Eqs.(3), (5), and (6) of the main text.

We would like to point out that the expressions for the shear rate and shear stress at the edge of the sample, Eqs.(5) and (6), differ from the commonly used expressions given in Gibson et al.[40] by the factors of $2^{-1/m}$ and 2^{-1}, respectively. We could not trace the origin of this discrepancy and used Eqs.(5) and (6) instead.

Acknowledgement

K. A. M. thanks EPSRC for PhD studentship funding with the Condensed Matter Centre for Doctoral Training (CM-CDT) under grant number EP/G03673X/1. Y. M. J. thanks the Indian National Science Academy and the Royal Society of Edinburgh for funding under their joint exchange program. P. S. C. thanks the ESPCI for funding as part of their Total and Joliot Chairs. We also thank Andrew Schofield for synthesizing the particles.

Supporting Information Available

Description of movie (pdf)

Z-stack of confocal images as a movie (avi)

References

(1) Cates, M. E.; Clegg, P. S. Bijels: a new class of soft materials. *Soft Matter* **2008**, *4*, 2132 – 2138.

(2) Lee, M. N.; Mohraz, A. Bicontinuous Macroporous Materials from Bijel Templates. *Advanced Materials* **2010**, *22*, 4836 – 4841.

(3) Lee, M. N.; Thijssen, J. H. J.; Witt, J. A.; Clegg, P. S.; Mohraz, A. Making a Robust Interfacial Scaffold : Bijel Rheology and its Link to Processability. *Advanced Functional Materials* **2013**, *23*, 417 – 423.

(4) Lee, M. N.; Santiago-Cordoba, M. A.; Hamilton, C. E.; Subbaiyan, N. K.; Duque, J. G.; Obrey, K. A. D. Developing Monolithic Nanoporous Gold with Hierarchical Bicontinuity Using Colloidal Bijels. *The Journal of Physical Chemistry Letters* **2014**, *5*, 809 – 812.

(5) Witt, J. A.; Mumm, D. R.; Mohraz, A. Microstructural tunability of co-continuous bijel-derived electrodes to provide high energy and power densities. *J. Mater. Chem. A* **2016**, *4*, 1000 – 1007.

(6) Herzig, E. M.; White, K. A.; Schofield, A. B.; Poon, W. C. K.; Clegg, P. S. Bicontinuous emulsions stabilized solely by colloidal particles. *Nature materials* **2007**, *6*, 966 – 971.

(7) Witt, J. A.; Mumm, D. R.; Mohraz, A. Bijel reinforcement by droplet bridging: a route to bicontinuous materials with large domains. *Soft Matter* **2013**, *9*, 6773 – 6780.

(8) Tavacoli, J. W.; Thijssen, J. H. J.; Schofield, A. B.; Clegg, P. S. Novel, Robust, and Versatile Bijels of Nitromethane, Ethanediol, and Colloidal Silica: Capsules, Sub-Ten-Micrometer Domains, and Mechanical Properties. *Advanced Functional Materials* **2011**, *21*, 2020 – 2027.

(9) Lee, M. N.; Mohraz, A. Hierarchically Porous Silver Monoliths from Colloidal Bicontinuous. *Journal of the American Chemical Society* **2011**, *133*, 6945 – 6947.

(10) Mohraz, A. Interfacial routes to colloidal gelation. *Current Opinion in Colloid and Interface Science* **2016**, *25*, 89 – 97.

(11) Cai, D.; Clegg, P. S.; Li, T.; Rumble, K. A.; Tavacoli, J. W. Bijels Formed by Direct Mixing. *Soft Matter* **2017**, *13*, 4824 – 4829.

(12) Cai, D.; Clegg, P. S. Stabilizing bijels using a mixture of fumed silica nanoparticles. *Chemical Communications* **2015**, *51*, 16984 – 16987.

(13) Haase, M. F.; Stebe, K. J.; Lee, D. Continuous Fabrication of Hierarchical and Asymmetric Bijel Microparticles, Fibers, and Membranes by Solvent Transfer-Induced Phase Separation (STRIPS). *Advanced Materials* **2015**, *27*, 7065 – 7071.

(14) Huang, C.; Forth, J.; Wang, W.; Hong, K.; Smith, G. S.; Helms, B. A.; Russell, T. P. Bicontinuous structured liquids with sub-micron domains using nanoparticle surfactants. *Nature Nanotechnology* **2017**, *12*, 1060 – 1063.

(15) Li, T.; Klebes, J.; Dobnikar, J.; Clegg, P. S. Controlling the Morphology Evolution of a Particle-Stabilized Binary-Component System. *Chemical Communications* **2019**, accepted, DOI: 10.1039/C9CC01519A.

(16) Erni, P. Deformation modes of complex fluid interfaces. *Soft Matter* **2011**, *7*, 7586 – 7600.

(17) Bai, L.; Fruehwirth, J. W.; Cheng, X.; Macosko, C. W. Dynamics and rheology of nonpolar bijels. *Soft matter* **2015**, *11*, 5282 – 5293.

(18) Rumble, K. A.; Thijssen, J. H. J.; Schofield, A. B.; Clegg, P. S. Compressing a spinodal surface at fixed area: the bijel in a centrifuge. *Soft Matter* **2016**, *12*, 4375 – 4383.

(19) Rotella, C.; Tence-Girault, S.; Cloitre, M.; Leibler, L. Shear-Induced Orientation of Cocontinuous Nanostructured Polymer Blends. *Macromolecules* **2014**, *47*, 4805 – 4812.

(20) Zhou, N.; Bates, F. S.; Lodge, T. P.; Burghardt, W. R. Shear flow behavior of a dynamically symmetric polymeric bicontinuous microemulsion. *Journal of Rheology* **2007**, *51*, 1027 – 1046.

(21) Liu, W.; Dong, X.; Zou, F.; Yang, J.; Wang, D.; Han, C. C. Rheological properties of polybutadiene/polyisoprene blend in the unstable and metastable regions under oscillatory shear. *Polymer (United Kingdom)* **2014**, *55*, 2744 – 2750.

(22) Huang, S.; Bai, L.; Trifkovic, M.; Cheng, X.; Macosko, C. W. Controlling the morphology of immiscible cocontinuous polymer blends via silica nanoparticles jammed at the interface. *Macromolecules* **2016**, *49*, 3911 – 3918.

(23) Domenech, T.; Velankar, S. S. Microstructure, phase inversion and yielding in immiscible polymer blends with selectively wetting silica particles. *Journal of Rheology* **2017**, *61*, 363 – 377.

(24) Zhang, H.; Yu, K.; Cayre, O. J.; Harbottle, D. Interfacial Particle Dynamics: One and Two Step Yielding in Colloidal Glass. *Langmuir* **2016**, *32*, 13472 – 13481.

(25) Bai, L.; He, S.; Fruehwirth, J. W.; Stein, A.; Macosko, C. W.; Cheng, X. Localizing graphene at the interface of cocontinuous polymer blends: Morphology, rheology, and conductivity of cocontinuous conductive polymer composites. *Journal of Rheology* **2017**, *61*, 575 – 587.

(26) Koumakis, N.; Petekidis, G. Two step yielding in attractive colloids: transition from gels to attractive glasses. *Soft Matter* **2011**, *7*, 2456 – 2470.

(27) Chan, H. K.; Mohraz, A. Two-step yielding and directional strain-induced strengthening in dilute colloidal gels. *Physical Review E* **2012**, *85*, 041403.

(28) Shao, Z.; Negi, A. S.; Osuji, C. O. Role of interparticle attraction in the yielding response of microgel suspensions. *Soft Matter* **2013**, *9*, 5492 – 5500.

(29) Zhao, C.; Yuan, G.; Han, C. C. Bridging and caging in mixed suspensions of microsphere and adsorptive microgel. *Soft Matter* **2014**, *10*, 8905 – 8912.

(30) Shukla, A.; Arnipally, S.; Dagaonkar, M.; Joshi, Y. M. Two-step yielding in surfactant suspension pastes. *Rheologica Acta* **2015**, *54*, 353 – 364.

(31) Shukla, A.; Arnipally, S.; Dagaonkar, M.; Joshi, Y. M. Yielding in Surfactant Suspension Pastes: Effect of Surfactant Type. *Journal of Surfactants and Detergents* **2016**, *19*, 999 – 1007.

(32) Hermes, M.; Clegg, P. S. Yielding and flow of concentrated Pickering emulsions. *Soft Matter* **2013**, *9*, 7568 – 7575.

(33) Primozic, M.; Duchek, A.; Nickerson, M.; Ghosh, S. Effect of lentil proteins isolate concentration on the formation, stability and rheological behavior of oil-in-water nanoemulsions. *Food Chemistry* **2017**, *237*, 65 – 74.

(34) Shaukat, A.; Sharma, A.; Joshi, Y. M. Squeeze flow behavior of (soft glassy) thixotropic material. *Journal of Non-Newtonian Fluid Mechanics* **2012**, *167-168*, 9 – 17.

(35) Chung, C.; Degner, B.; McClements, D. J. Instrumental mastication assay for texture assessment of semi-solid foods:. *Food Research International* **2012**, *49*, 161–169.

(36) Joshi, Y. M.; Petekidis, G. Yield stress fluids and ageing. *Rheologica Acta* **2018**, *57*, 521 – 549.

(37) Covey, G. H.; Stanmore, B. R. Use of the parallel-plate plastometer for the characterisation of viscous fluids with a yield stress. *Journal of Non-Newtonian Fluid Mechanics* **1981**, *8*, 249 – 260.

(38) Adams, M. J.; Edmondson, B.; Caughey, D. G.; Yahya, R. An experimental and theoretical study of the squeeze-film deformation and flow of elastoplastic fluids. *Journal of Non-Newtonian Fluid Mechanics* **1994**, *51*, 61 – 78.

(39) Yan, Y.; Zhang, Z.; Cheneler, D.; Stokes, J. R.; Adams, M. J. The influence of flow confinement on the rheological properties of complex fluids. *Rheologica Acta* **2010**, *49*, 255 – 266.

(40) Gibson, A. G.; Kotsikos, G.; Bland, J. H.; Toll, S. In *Rheological Measurement*; Collyer, A. A., Clegg, D. W., Eds.; Chapman and Hall, 1998; pp 550 – 592.

(41) Engmann, J.; Servais, C.; Burbidge, A. S. Squeeze flow theory and applications to rheometry: A review. *Journal of Non-Newtonian Fluid Mechanics* **2005**, *132*, 1 – 27.

(42) White, K. A.; Schofield, A. B.; Wormald, P.; Tavacoli, J. W.; Binks, B. P.; Clegg, P. S. Inversion of particle-stabilized emulsions of partially miscible liquids by mild drying of modified silica particles. *Journal of Colloid and Interface Science* **2011**, *359*, 126 – 135.

(43) Imhof, A.; Megens, M.; Engelberts, J. J.; de Lang, D. T. N.; Sprik, R.; Vos, W. L. Spectroscopy of Fluorescein (FITC) Dyed Colloidal Silica Spheres. *The Journal of Physical Chemistry B* **1999**, *103*, 1408 – 1415.

Graphical TOC Entry